CFD Simulation of Airflow in a 17-Generation Digital Reference Model of the Human Bronchial Tree

T. Gemci[a,b,*], V. Ponyavin[a], Y. Chen[a,b], H. Chen[a], and R. Collins[b]

[a]*Nevada Center for Advanced Computational Methods (NCACM)*
[b]*Biomedical Engineering Program, Mechanical Engineering Department,*
University of Nevada, Las Vegas (UNLV)
4505 Maryland Pkwy, Box: 454027, Las Vegas, NV 89154, USA
[*]*Corresponding author:*
Tel: +1 (702) 895 2338; Fax: +1 (702) 895 1860; Email: tgemci@nscee.edu (T. Gemci)

Abstract
Computational fluid dynamics (CFD) studies of airflow in a digital reference model of the 17-generation airway (bronchial tree) were accomplished using the FLUENT® computational code. The computational mesh was based on the anatomical graph data of a digital reference model by Schmidt *et al.* (2004) derived from High-Resolution Computer Tomography (HRCT) imaging of an *in vitro* preparation in which specially adapted image processing algorithms were applied to delineate and segment the bronchi. The 17-generation airway model containing 1453 bronchi was developed for the pressure drop and flow field studies. The lung model consists of $6.744 \cdot 10^6$ unstructured tetrahedral computational cells. A steady-state airflow rate of 28.3 L/min was used to simulate the transient turbulent flow regime using a Large Eddy Simulation (LES) turbulence model. This CFD mesh represents the somewhat irregular but anatomically realistic asymmetrical branching pattern of the larger airways, leading to varied airway lengths and cross-sectional areas. It is demonstrated that the nature of the secondary vortical flows which develop in such asymmetric airways varies with the specific anatomical characteristics of the branching conduits.

Keywords: Pulmonary airways; Human pulmonary airway model; Asymmetric bronchial tree; computational; LES model

1. Introduction

The uptake of particulate matter by inhalation leads to complex transport processes influenced by unsteady convection through a non-dichotomously branching network of conducting conduits (airways). The properties of the particulate matter (its particle geometry, diameter and density distributions, and its affinity to adhere to the mucous linings of the conduits) play a crucial role in the subsequent uptake by, and deposition pattern within, the pulmonary tract. While the respiratory tract may be the target organ of concern with regard to many pollutants, for others it is merely one of several possible routes of entry into the body. Furthermore, the pulmonary flow features are closely related to the anatomical details of the branching network of some 23 generations of pulmonary airway conduits.

A widely used model for CFD simulations and predictions of gas transport, particle deposition and dosimetry is that characterized by a regular, dichotomous branching pattern [Synder *et al.* (1981), Zhao and Lieber (1994), Cala*y et al.* (2002), Lee and Lee (2002), Liu *et al.* (2003), Kleinstreuer and Zhang (2003), Nowak *et al.* (2003), Shi *et al.* (2004), Zhang and Kleinstreuer (2004)], a representation that has its origin in the so-called trumpet model of Weibel (1963), who measured the dimensions of

airway branches of a human lung distally to generation G4. Thereafter, his measurements were less complete down to generation G10, where only 10% of the branches were measured. Weibel's study was used to develop the widely used symmetric model "A" corresponding to regular dichotomy. Nowak *et al.* (2003) and Cebral and Summer (2004) used CT scans to characterize the pulmonary airways more realistically, albeit only down to the 4^{th} generation subunit (G0 to G4). Kriete *et al.* (2004) reported in a conference paper the oxygen gas transport and particle deposition in a digital reference model based on data by Schmidt *et al.* (2004) with a limited 29-terminal bronchi outlet; whereas, our study has been based on the same data of Schmidt *et al.* (2004) but includes all 720 bronchi outlets. Their final mesh of Kriete *et al.* contained a total of 456,463 prism and tetrahedral elements using the ICEM CFD software package.

Calay *et al.* (2002) studied the respiratory flow patterns in a single first generation bifurcation distal to the trachea and in a multiple-bifurcation model, with their three generations based on the anatomy given by Horsfield *et al.* (1971). They used four different grid densities varying comprising respectively 31104, 79820, 159872 and 320980 nodes. Lee and Lee (2002) generated a 3-D conduit network model with four generations which conformed closely to Weibel's 1963 model in order to study aerosol bolus dispersion. The total number of cells in their 90° out-of-plane model ranged from 40,000 to 60,000. Liu *et al.* (2003) studied the 3-D inspiratory flow in a 3-generation asymmetric lung airway model from the 5^{th} to the11^{th} branches of Weibel's model "B", corresponding to an irregular dichotomy. They used 123,591 tetrahedral elements for the unstructured mesh of the pulmonary airway. Kleinstreuer and Zhang (2003) analyzed targeted aerosol drug deposition analysis in a rigid triple-bifurcation pulmonary airway model. Their model represents the symmetrically bifurcating generations G3 to G6 as in Weibel's lung model with three different hemispherical tumor models placed along the side wall of the G5 airway. Their final mesh comprised about 360,000 cells for the triple bifurcation configuration. Nowak *et al.* (2003) demonstrated a four-subunit CFD simulation method for the human tracheobronchial tree. They elected to economize on computational effort by segmenting the first 12 generations into four 3.5-generation "tranches" or subunits (G0-G3, G3-G6, G6-G9, and G9-G12), without adequately accounting for the fluctuation in boundary conditions between each tranche or subunit. Additionally, they compared the simulated Weibel-based anatomical model to the more realistic CT scan-based anatomical model with a 4-generation subunit. They imported the CT scan-based lung image of Sauret *et al.* (1999) as a surface mesh up to 9 generations. Their results indicate dramatic differences in the predicted particle deposition patterns between the two models. The absence of airway curvature and surface irregularities in a Weibel-based model renders the flow fields very different from those in a real human lung (CT-based model). Shi *et al.* (2004) have studied the nanoparticle deposition in bifurcating tubes of a 3-generation model (G3-G5 Weibel's pulmonary airway model) for both planar and non-planar geometries. They used 892,008 computational cells for the planar G3-G5 pulmonary airway model and 845,000 for the non-planar one. Zhang and Kleinstreuer (2004) recently studied nanoparticle deposition in a human upper airway model consisting of two connected segments of a simplified human cast replica extending from the mouth to the trachea (generation G0), as adapted from a human cast and continuing with symmetric bifurcations over generations G0 to G3, based upon Weibel's model. They used 420,000 computational cells for the oral airway and 670,000 cells for the four-generation pulmonary airway model. Cebral and Summer (2004) studied the central tracheal and bronchial airways down to 4 generations by using a virtual bronchoscopy reconstruction method. Airflow patterns resulting from airway stenoses in generations from G0 to G4 were simulated computationally. van Ertbruggen *et al.* (2004) studied the gas flow and particle deposition in a realistic 3D model of the bronchial tree, extending from the trachea to the segmental bronchi (7^{th} airway generation for the most distal airways). Their model was based on the morphometrical data of Horsfield *et al.* (1971).

Realistic physical morphometry, incorporating a large number of generations, is essential for adequately simulating fluid and particle dynamics in human pulmonary airways. In recent years, there have

been several published research works [Kitaoka *et al.* (1999), Tawhai *et al.* (2000 and 2004), Spencer *et al.* (2001), Tgavalekos *et al.* (2003), Sera *et al.* (2003), and Schmidt *et al.* (2004)] focusing on the generation of pulmonary airway models using both mathematical algorithm development and new experimental imaging techniques. Kitaoka *et al.* (1999) introduced a 3D model of the human airway tree down to the terminal bronchioles which was generated by a deterministic algorithm that incorporated duct branching and space division. Tawhai *et al.* (2000 and 2004) developed a 3-D tree-growing algorithm for generating conducting airway models specific to a given host geometry. The host geometrical surface was derived from Magnetic Resonance Imaging (MRI). They included 29,445 terminal bronchioles in their model. Spencer *et al.* (2001) developed a dynamic surface modeling technique based on data from idealized models (Weibel's model with symmetric, dichotomously branching morphology) to construct 3-D computer simulations of tubular pulmonary airway structures within lungs extending from the trachea (Generation G0) to the alveoli (Generation G23). Sera *et al.* (2003) developed a two-step method to visualize small airways in detail by staining the lung tissue with a radio-opaque solution and then visualizing the tissue with a cone-beam microfocal X-ray Computed Tomography (CT) system. They employed the Staining and CT (SCT) imaging method to stain and visualize excised rodent pulmonary airways.

Tgavalekos *et al.* (2003) have advanced the 3-D airway tree model of Kitaoka *et al.* (1999) to predict pulmonary function on the basis of airway structure, particularly when constriction patterns are imposed heterogeneously on the pulmonary tree in specific anatomic locations. They also introduced pulmonary function into a 3-D model which allows specific control of anatomical regions, and compared their model predictions with ventilation images obtained from Positron Emission Tomography (PET) and measurements of dynamic mechanical pulmonary function. They generated 50,400 computational airway cells with their model.

2. Current 17-generation anatomical model

We have based our present CFD analysis on the best published anatomically explicit human lung model available to date; i.e. the 17-generation anatomical model developed by Schmidt *et al.* (2004). Fig. 1 depicts their bronchial tree models as derived from High-Resolution Computed Tomography (HRCT) imaging of an *in vitro* preparation. Their model data represent the anatomy of the human lung of an adult male, free of pathological alterations. Fig. 1a portrays a realistic 3D surface representation of the segmented volume of the bronchial tree. The cartilaginous rings can be observed in the main upper generations. The conduit model reconstructed from an abstracted and adapted topological graph, as shown in Fig. 1b, contains 1453 bronchi up to the 17^{th} Horsfield order. To the authors' knowledge, the computational study described herein represents the first published CFD simulation of the airflow in a digital reference model up to a maximum 17 generations of the human pulmonary airways with 1453 bronchi. The entire human lung is comprised of some 26 generations of branching pulmonary airway conduits. The computer-generated symmetric human lung model of Spencer *et al.* (2001) for the 23-generation tree does not possess the detail required for the current computational investigation and is not as accurate as the Schmidt *et al.* (2004) anatomical airway model.

3. CFD simulation

The characterization of the anatomy and morphometry of the airways constitutes the first step in an examination of the respiratory flow field and aerosol deposition. Our characterization of the anatomy of airways must be sufficiently realistic, as we intend to focus in subsequent studies with extensions of the present model on techniques to provide more efficient delivery of inhaled medications and to understand better the effects of inhaled pollutants. Indeed, fine particle diffusion within the human airways plays a critical role in aerosol therapy and inhalation toxicology. Particle deposition patterns in

the branching pulmonary network are highly influenced by the irregular and asymmetric branching structures of the human lung. These detailed anatomical considerations will have important implications for risk assessment programs and aerosol therapy protocols.

In this study, the homogenous airflow in a comprehensive digital reference model of up to maximum 17 generations pulmonary airway tree was computed using the commercial CFD code FLUENT® (version 6.1.18). This quasi steady-state model will subsequently be extended in future works to evaluate the convection and diffusion of particular distributions of inhaled particles and aerosols to various sites within the pulmonary airways. The computational mesh was generated using the FLUENT mesh generation code GAMBIT®. FLUENT employs a finite-volume method to solve the Navier-Stokes and continuity equations on an arbitrarily shaped flow domain with appropriate boundary conditions. It also provides for various turbulence models, such as two-parameter models (k-ε and k-ω) as well as for LES (Large Eddy Simulation). Our computations were performed on two different platforms: 1) RackSaver® RS-1100 Cluster with 13 GB of RAM and with 13 Dual (2x) Intel® Pentium® III processors at 1.26 GHz in the NSCEE (National Supercomputing Center for Energy and Environment) of the University of Nevada Las Vegas (UNLV) and 2) a tera-scale computing system which comprises 750 Compaq Alphaserver ES45 nodes, each of which contains four 1-GHz processors in the PSC (Pittsburgh Supercomputing Center). The steady-state solution of the flow field was assumed to have converged when the residuals reduced to less than 10^{-4}. A typical run time was approximately 50 hours on the NSCEE machine.

In this CFD study of airflow in our human pulmonary tree model, computations were performed at 28.3 L/min for a quasi steady-state volumetric adult inhalation flow rate and as well as at 6, 12, 18, 24, and 30 L/min for the study of static pressure variation.

3.1 Human Bronchial Tree Model and Mesh Generation

The computational mesh is generated using GAMBIT® software, after transporting into it the abstracted topological graph data from Schmidt *et al*. (2004). These graphical data contain all the information required to reconstruct a simplified, tube-like surface representation of the geometry, as shown in Fig. 1b. This tube-like surface representation still retains the exact anatomical asymmetry and branching angles. For the digital reference up to a maximum 17-generation pulmonary airway tree model, we generated a large, reasonable yet computationally affordable mesh size consisting of $6.744 \cdot 10^6$ unstructured tetrahedral cells as is shown in Fig. 2. The mesh generation file is 660 MB in size and takes 1 hour to develop on the terascale machine of PSC. The inlet and outlet boundary sections are placed in GAMBIT® before importing the data into FLUENT®.

3.2 Numerical Methods

The computational mesh models of the human pulmonary tree were then imported into Fluent [Fluent 6.1.18, Fluent Inc., (2003)]. The steady-state mass conservation (Eq. 1) and momentum equations (Eq. 2) were solved using a finite-volume method to compute the particle-free fluid flow field. Air was assumed here to be a homogenous, Newtonian fluid with constant density ρ and viscosity μ. The governing flow equations (continuity and momentum) for the air density ρ and flow velocity $\vec{\mathbf{v}}$ are given as

$$\frac{\partial \rho}{\partial t} + \nabla \cdot \left(\rho \vec{\mathrm{v}}\right) = S_m \tag{1}$$

where the source term S_m is the mass added to the continuous phase from the dispersed second phase.

$$\frac{\partial}{\partial t}(\rho\vec{v}) + \nabla\cdot(\rho\vec{v}\vec{v}) = -\nabla p + \nabla\cdot\left(\mu\left[\left(\nabla\vec{v} + \nabla\vec{v}^{\mathrm{T}}\right) - \frac{2}{3}\nabla\cdot\vec{v}I\right]\right) + \rho\vec{g} + \vec{F} \qquad (2)$$

where p is the static pressure, and $\rho\vec{g}$ and $\vec{F}$ are the gravitational body force and external body forces, respectively. The second term on the right hand side is the stress tensor in which $\nabla\vec{\mathbf{v}}^{\mathrm{T}}$ denotes the transpose of the Laplacian of $\vec{\mathbf{v}}$, while I is the unit tensor.

In order to model the turbulent air flow, the LES (Large Eddy Simulation) model was used in the current airflow study. In LES, large energy–containing eddies are computed directly, while the remaining smaller eddies are modeled using a subgrid-scale (SGS) turbulence model. By contrast, RANS (Reynolds-Averaged Navier-Stokes)-based turbulence modeling is an approach in which an entire range of scales is modeled together in a single entity. More details on the implementation of this turbulence model are available in the FLUENT® documentation (Fluent, Inc., 2003).

3.3 Boundary Conditions

The quasi steady-state inlet velocity is taken here as 2.896 m/s, based on a tracheal inlet area of 162.86 mm^2 and a tracheal diameter of 14.4 mm. The inflow boundary condition with a uniform inlet

velocity field is applied at the tracheal inlet section (generation G0). The outflow boundary condition is widely chosen in many CFD analyses of pulmonary airflows because the pressure at each outlet (total of 720 outlets for the digital reference model of lung bronchial tree up to a maximum 17 generations employed here) must be known *a priori*. Its determination should reflect the effect of the remaining truncated generations G18 through G26 at the alveolar level. Such inflow and outflow boundary conditions have been incorporated in many CFD models of the pulmonary airways [see Calay *et al.* (2002), Kleinstreuer and Zhang (2003) and Nowak *et al*. (2003)]. Nowak *et al.* (2003) have also demonstrated that the predicted in-plane velocity vectors at the midpoint of G4 for the two sets of boundary conditions (pressure outlets and uniform outflows) possess similar velocity fields.

We used an inflow boundary condition at G0 and outflow boundary conditions at all terminal bronchi exits (720 outlets for our digital reference lung model. Details are provided in the following section. The total mass flow rate at all bronchial exits is very close to the inlet value with a very small difference on the order of $11.2\cdot10^{-6}$ g/sec. This mass flow difference is less than 0.002% of the inlet mass flow rate calculated from $\left(\dot{m}_{in} - \dot{m}_{out}/\dot{m}_{in}\right)\cdot 100$. No-slip boundary conditions were assumed at the pulmonary airway walls. Generation G0 and the first bifurcation were represented by a less dense mesh ($1.063\cdot10^6$ tetrahedral cells) than for the remainder generations (up to a maximum 17 generations) of modeled airways ($5.680\cdot10^6$ unstructured tetrahedral cells) as the flow was more uniform at this upstream location. The computational mesh with a total of $6.744\cdot10^6$ cells was divided into $1.063\cdot10^6$ tetrahedral cells in the G0 zone and into $5.680\cdot10^6$ unstructured tetrahedral cells in the remaining zones.

4. Results and discussions

4.1. Pulmonary Model up to a Maximum 17 Generations

Preliminary CFD calculations were conducted for the digital reference pulmonary airway model in order to validate our specification of assigned pressure drop across successive bifurcations. The airflow calculation has been carried out using the LES turbulence model. The turbulence modeling in the upper airway generations is very important, especially for the future determination of particle deposition. During inhalation, the flow transitions from laminar to turbulent flow in the larynx and in the tracheal section, and continues into the first main generation. The conducting zone contains the trachea, bronchi, bronchioles, and the terminal bronchioles. In this zone, there is no gas-blood exchange. There is an increase in aggregate cross-sectional area as the conduits become narrower. This increase in cross-sectional area causes a drop in airway pressure and a corresponding drop in flow rate, such that final air-blood exchange occurs by diffusion at the alveolar level. Our CFD calculations, as described further below, indicate that the static pressure drop is 50 Pa for a volumetric gas flow rate of 28.3 L/min over the complete span of the up-to-a-maximum 17 generation airways as shown in color-coded Fig. 3.

Pressure drop in the bifurcating airways plays an essential role in the respiratory process. The resistance of an airway, group of airways, or the whole lung is defined as the pressure drop between its ends divided by the flow rate though it. In general, the airway network resistance will vary with lung volume as the airway dimensions change with the overall flow rate $\dot{Q}_g$ into (and out of) the lung, because of the nonlinear fluid mechanical effects previously described. The pressure and velocity in the airways also vary from point to point. Secondary flows in the pulmonary airways can be very pronounced. Pedley *et al.* (1971) and Pedley (1977) determined the static pressure variation along the airway tree based on the energy equation. The static pressure drop was predicted as 60 Pa along Weibel's symmetric bronchial tree at an inspired flow rate of 60 L/min (1000 cm^3/sec) [ref: Fig. 11 on page 262 of Pedley (1977)], which is in reasonably good agreement with the experimental measurement by Hyatt and Wilcox (1963) of a pressure drop of 75 Pa across the entire respiratory tract. Much more complex analysis is required for asymmetric branching because the flow in each branch then depends on the resistance in every other branch, both proximally and distally, which would require the solution of 10^{20} simultaneous equations. Our comprehensive 3-D CFD simulation of the asymmetric bronchial tree model predicted a reasonable static pressure drop of 50 Pa across the up-to-a-maximum 17-generation digital reference model for a steady-state flow rate of 28.3 L/min, corresponding to normal adult breathing conditions. We also obtained the variation of the viscous pressure over the complete span of the up-to-a-maximum 17 generations of airways as a function of 5 additional gas flow rates of 6, 12, 18, 24, and 30 L/min (corresponding to 100, 200, 300, 400, and 500 cm^3/s, respectively). The viscous pressure drop increases nonlinearly from 6 Pa at 100 cm^3/s to 54 Pa at 500 cm^3/s, as shown in Fig. 4. This nonlinearity of the pressure-flow rate relationship was also observed and predicted by Pedley [see Fig. 11 in Pedley (1977)].

The viscous pressure drop over two selected airway path-lines is shown in Fig. 5. Path-line #1 is chosen in the left lung whereas the path-line #2 lies in the right lung for an overall pulmonary flow rate of 28.3 L/min. The local pressure drops are different because of the anatomical asymmetries between right and left lungs along the two selected path-lines. For example, the viscous pressure drop is 34 Pa through the first 5 generations in path-line #1; whereas it is 15 Pa across the first 5 generations in path-line #2. Furthermore, a pressure drop of 49 Pa is reached in the 11^{th} generation for path-line #1; whereas this value is not attained until the 16^{th} generation for path-line #2 of the right lung. There is also a clearly visible zigzag trend of decrease and increase for the first 6 generations in path-line #1; whereas the same trend obtains for the first 9 generations in path-line #2. The same trend is also noted in the literature for a CFD simulation of 7 generations (see Fig. 8 in van Ertbruggen *et al*. 2005 and as well as in the formula for airway pressure drop of Pedley 1977).

Calculation of flow partitioning in the lung is essential because of anatomical asymmetry of the right and left lungs and its effect on aerosol deposition. Fig. 6 depicts the percentage change in mass flow rate in the first three generations of the right and left lungs. For example, in the second generation where

the main bronchus subdivides into two secondary bronchi (right lung bronchi are shown as G5 while the left lung counterparts are shown as G2). The mass flow rate in G5 is 67.2%, but in G2 only 32.8% of the flow rate in the main G1 bronchus, corresponding to a ratio of mass flow rates (G5/G2) of 2.04. A similar trend can also be seen in the third generation of the left lung (G3/G4 = 1.22) and in the right lung (G6/G7 = 2.28). Generally, the lateral daughter branch attracts much more fluid flow than does the medial branch, as was also observed in the asymmetric pulmonary airway simulation by Liu *et al.* (2003).

4.2 Airflow Velocity Fields

Airflows in the upper airways can periodically exhibit the characteristics of laminar, transitional, or fully developed turbulent flow. Changes in the flow regime can be rapidly affected during inhalation due to a succession of conduit cross-sectional area changes occurring between the trachea and the respiratory surfaces of the lungs. The velocities in the pulmonary airways are very low and decrease further as the airflow passes through the smaller airways deep into the pulmonary bronchioles.

A uniform velocity profile was imposed computationally at the inlet to the trachea with an average value of 2.896 m/s, corresponding to a steady-state inhalatory flow rate of 28.3 L/min and a tracheal diameter of 14.4 mm. At normal breathing rates of 28.3 L/min, the airflow in the larynx and in the tracheal section of the upper airways is slightly turbulent. Distal to the first few main upper generations, the airflow quickly becomes laminar-turbulent transition flow. The effects of the turbulent laryngeal jet on the gas flow field extend throughout the length of the larynx and cause recirculatory flows and turbulent eddies which are likely to persist even beyond the tracheal bifurcations (Gemci *et al.,* 2002, 2003). Stapleton *et al.* (2000) and Allen *et al.* (2004) have shown that the choice of a specific turbulent model is critical for accurate predictions of subsequent particle deposition in the upper respiratory tract. For this reason we performed our airflow simulation with the LES turbulent model, even though it is computationally more expensive than RANS-based turbulence models. The uniform inlet velocity profile of 2.896 m/s at the tracheal inlet section begins to develop into a non uniform velocity profile and attains a velocity of 3.5 m/s at the midline of the trachea proximal to the first bifurcation. Immediately distal to the tracheal bifurcation, the flow in the right bronchus is higher than in the left one due to their different diameters, different lengths and asymmetric structures.

The velocity fields in more realistic pulmonary airway models are more complicated than those in the Weibel-based symmetric or asymmetric models. Airway curvature and complex shapes at junctions contribute to those complex flow patterns as stated in Novak *et al.* (2003). Figs. 7 and 8 show the secondary flow patterns in the main left and right bronchi. In previous Weibel-based airway bifurcation models, the secondary flow seen in the in-plane cross-section of the bronchus was directed from the center of the inner wall towards the center of the outer wall; it then divided equally into a double vortex, also known as Dean flow. The Dean flow pattern was also observed in the daughter branches following the bifurcation of a mother branch in both symmetric and asymmetric Weibel-based pulmonary airway models [Pedley *et al.* (1971), Guan and Martonen (2000), Calay *et al.* (2002), Zhang *et al.* (2002), Liu *et al.* (2003), Nowak *et al.* (2003), and Shi *et al.* (2004)]. 29. Weibel, E.R., 1963. *Morphometry of the Human Lung*, Springer Verlag, Berlin.

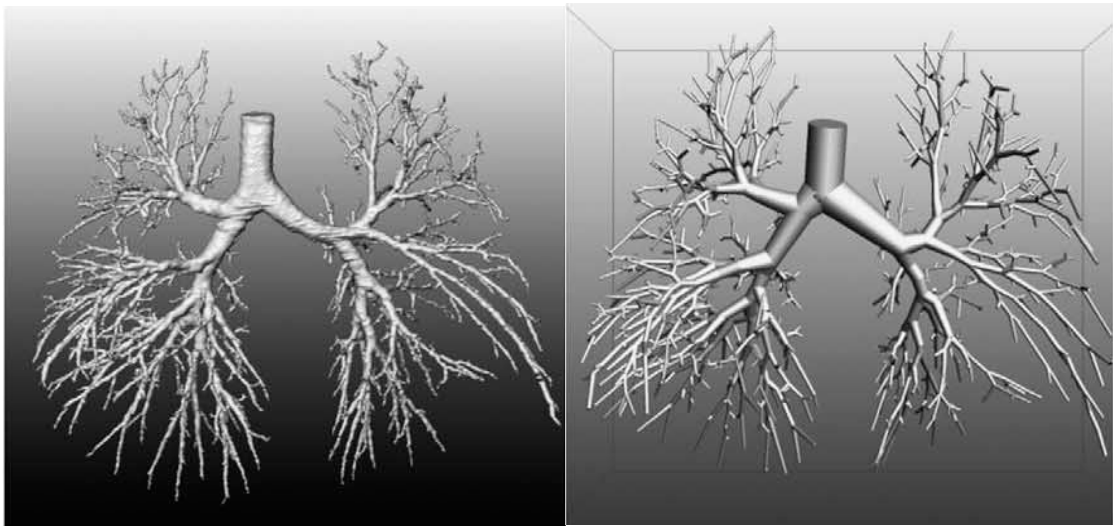

(a) (b)

Fig. 1 3D anterior visualization of bronchial tree models from Schmidt *et al*., 2004.
(a) Surface representation of segmented volume data; (b) Visualization of a tube model reconstructed from abstracted topological graph data. Reprinted by permission of Elsevier Ltd.

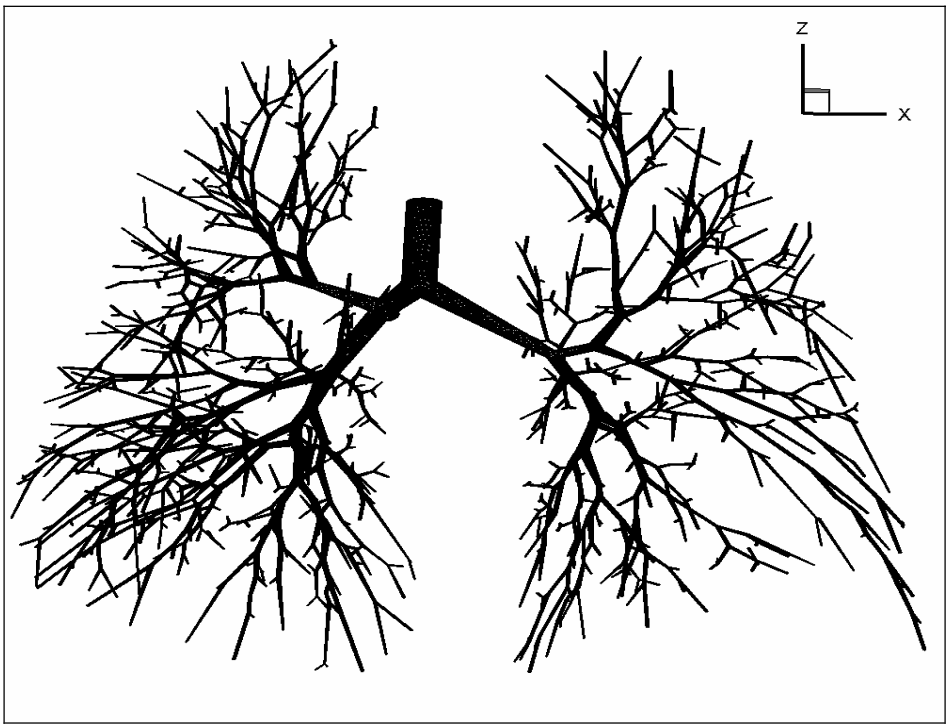

Fig. 2 Anterior view of generated mesh of 17 generations of pulmonary airways (1453 bronchi) with $6.744 \cdot 10^6$ unstructured tetrahedral cells based on abstracted topological graph data from Schmidt *et al*., 2004 [1]. The computational cells cannot be seen in this image.

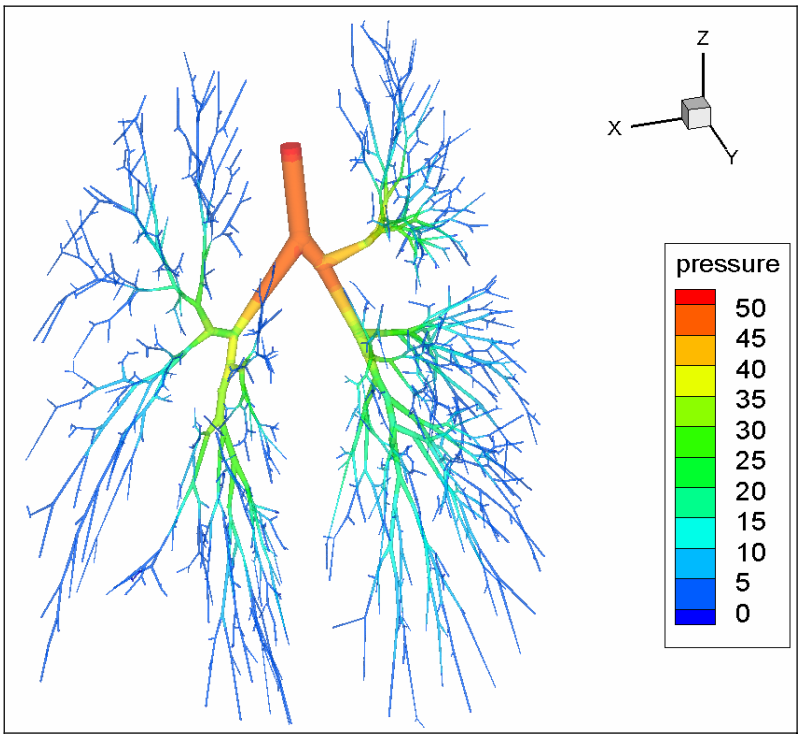

Fig. 3 Pressure distributions across the 17-generation bronchial tree model (posterior view) for a volumetric gas flow rate of $\dot{Q}_g = 471.66$ cm^3/s (28.3 L/min).

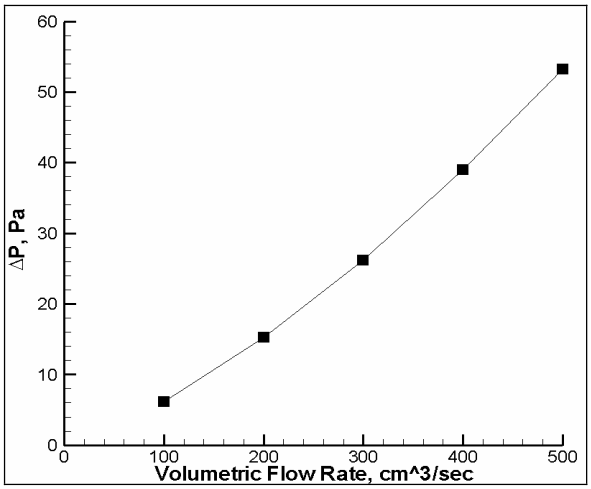

Fig. 4 Pressure drop across the 17-generation bronchial tree model as a function of volumetric gas flow rate from 100 to 500 cm^3/s (6 to 30 l/min, respectively).

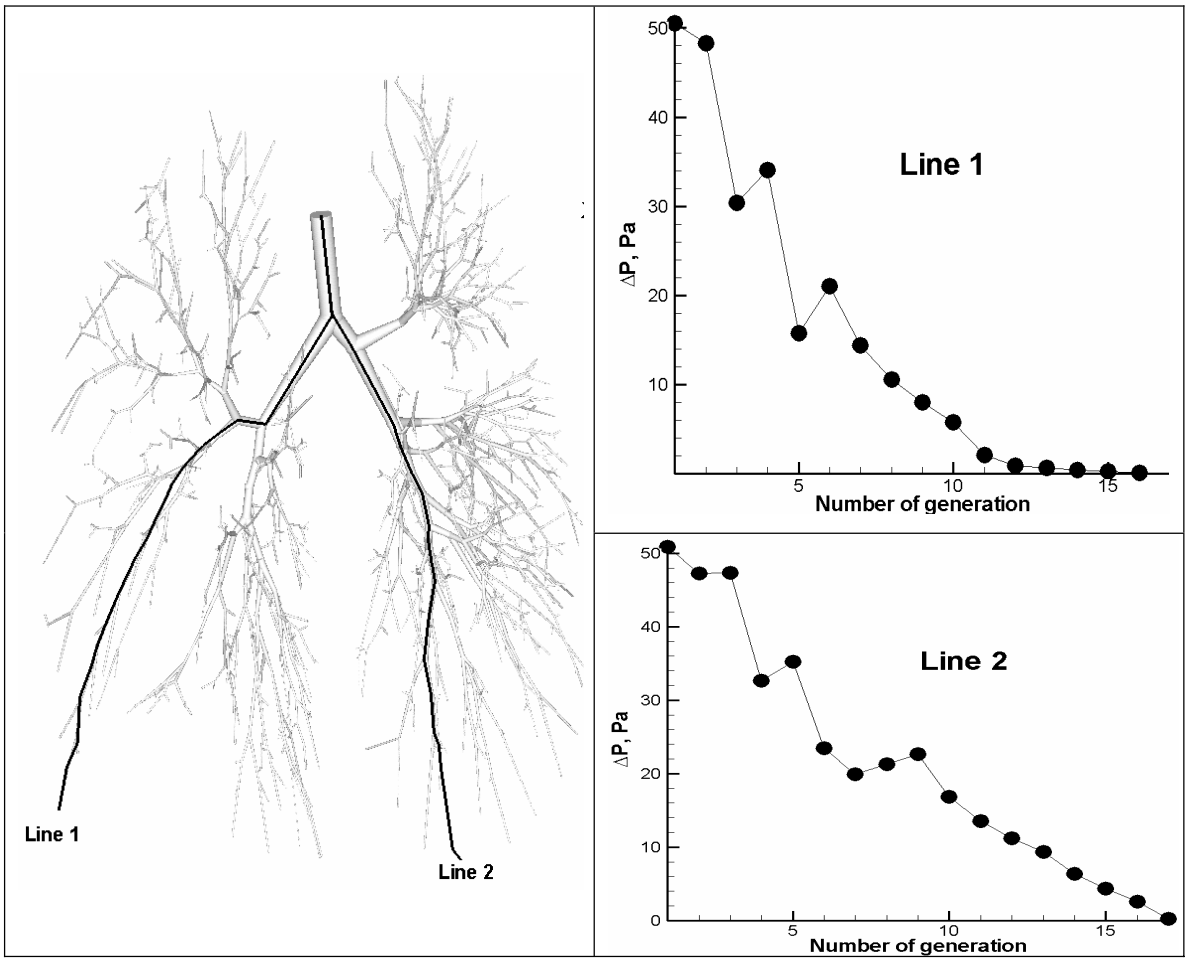

Fig. 5 Variation of the pressure drop along two selected path lines for a flow rate of 28.3 L/min.

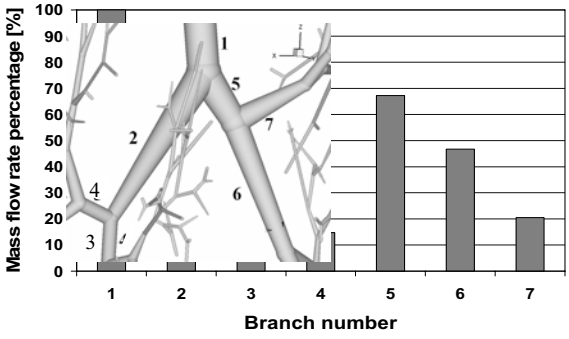

Fig 6 Percentage variations of the mass flow rate portioning in the first main bifurcation and in its distal daughter branches. Total mass flow rate is 0.6125 g/s (corresponding 500 cm^3/s or 30 L/min)

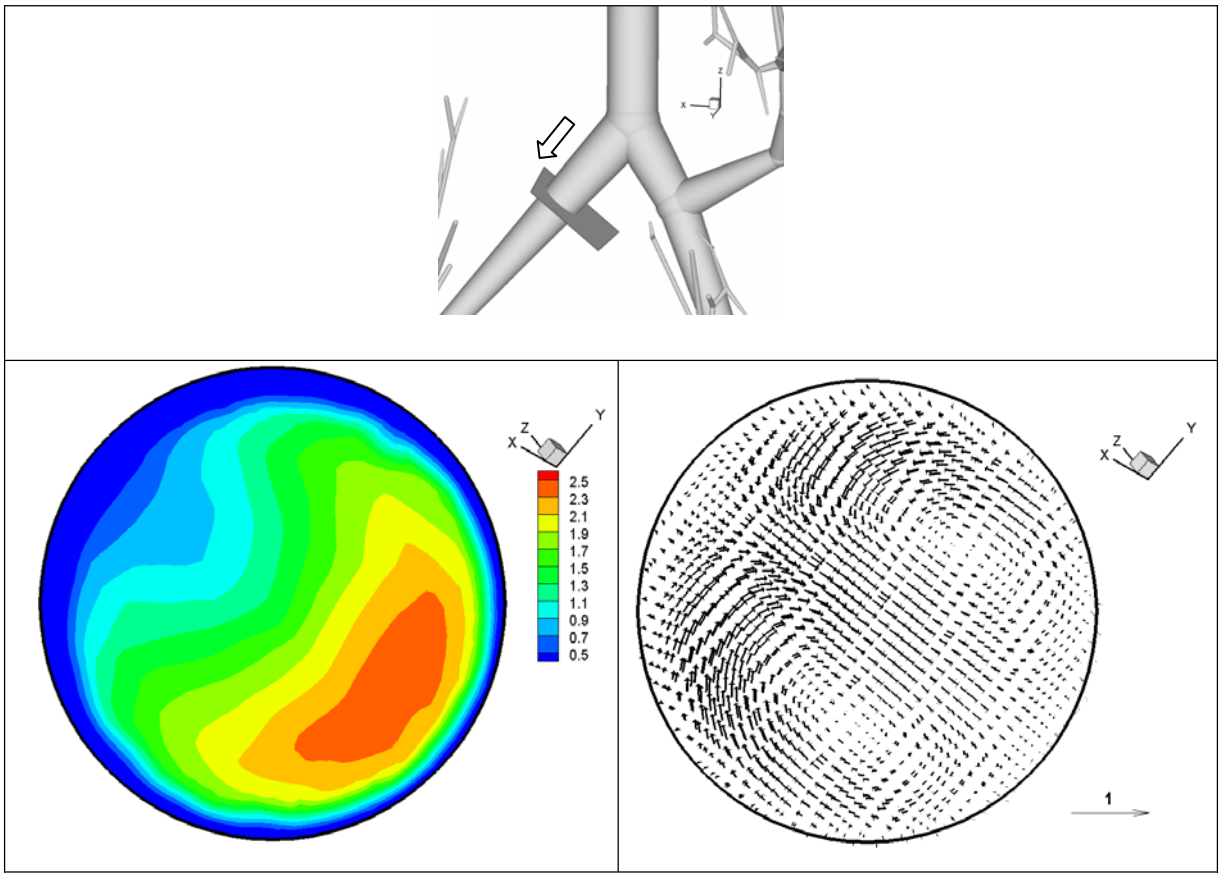

Fig. 7 The velocity vector (right frame) and velocity magnitude (left frame) are shown at an in-plane cross-section at the left main bronchus shown on the top frame. Pictured here is an oblique plane view of the first left bronchus in a direction perpendicular to the flow.

5. Conclusions

Computational fluid dynamic (CFD) evaluations of the quasi-steady homogeneous airflow in the human respiratory tract have been presented here with a view to their subsequent application to the study of the uptake of particulate matter by the pulmonary airways in flows varying periodically in time.

Capture of a realistic anatomical model of the complete pulmonary branching conduits is complex but essential for the successful development of an airflow model, along with a functional numerical scheme. To this end, we have adapted the recent anatomical graph data of Schmidt *et al.* (2004) within the framework of up to a maximum 17-generation bifurcating pulmonary airway tree of the human lung, based on measurements derived from High-Resolution Computer Tomography (HRCT). Assumed pressure drops across successive bifurcations have been shown to agree reasonably well with other indications derived from earlier published results using more limited anatomical models. Laminar-turbulent flow transitions have been accounted for with a LES model. The flow fields resulting from this comprehensive computational formulation also reflect to a certain extent the development of secondary swirling flows similar to those resulting from airway curvature.

This digital reference model of the human lung tree is proposed as a first step toward the development of detailed time-varying fine-particle deposition models with a view to the quantitative

design and assessment of therapeutically targeted drug delivery systems via the respiratory tract and to the regional evaluation of the ingestion of particulate pollutants into the lung.

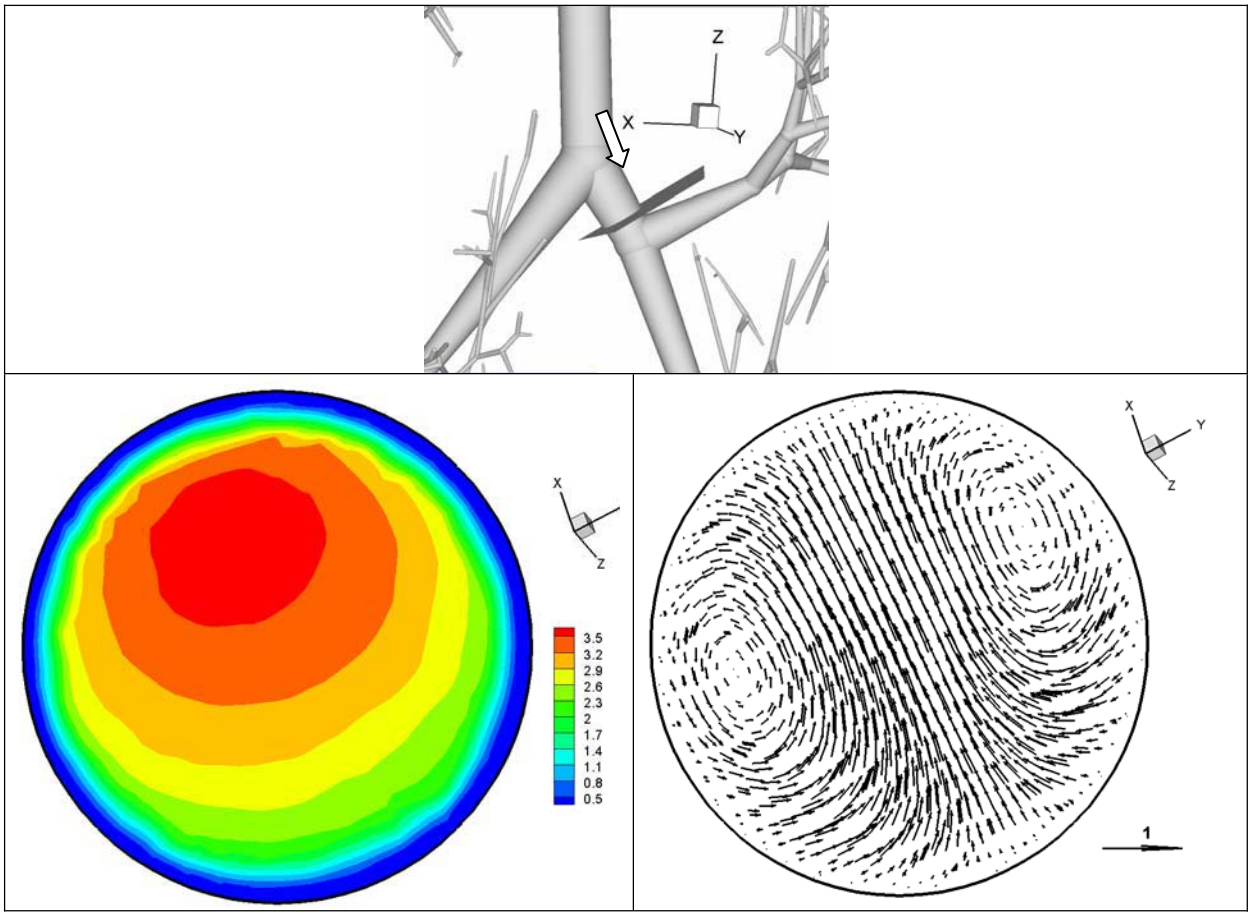

Fig. 8 The velocity vector (right frame) and velocity magnitude (left frame) are shown at an in-plane cross-section at the right main bronchus shown on the top frame. Pictured here is an oblique plane view of the first right bronchus in a direction perpendicular to the flow.

Acknowledgements

We express our thanks to Dr. Andres Kriete at the Coriell Institute for Medical Research, Camden, NJ and to his co-authors for providing us the abstracted topological graph data of the human bronchial tree model. The use of FLUENT and access to the supercomputers at the National Supercomputing Center for Energy and Environment (NSCEE at UNLV – University of Nevada, Las Vegas, USA) and the Pittsburgh Supercomputing Center (PSC in Pittsburgh, Pennsylvania, USA) under grant number CTS010015P) are also gratefully acknowledged.

Rererences

1. Allen, G.M., B.P. Shortall, T. Gemci, T.E. Corcoran, and N.A. Chigier, 2004. Computational simulations of airflow in an *in vitro* model of the pediatric upper airways. *ASME Journal of Biomechanical Engineering*, **126**:604-613.
2. Calay, R.K., Kurujareon, J., and Holdø, A.E., 2002. Numerical simulation of respiratory flow patterns within the human lung. *Respiratory Physiology & Neurobiology*, **130**:201-221.
Cebral, J.R. and Summer, R.M., 2004. Tracheal and central bronchial aerodynamics using virtual bronchoscopy and computational fluid dynamics. *IEEE Transactions on Medical Imaging*, **23**(8):1021-1023.
3. Fluent Inc., 2004. *Fluent 6.1.18 User's Guide*, Lebanon, NH.
4. Fung, Y.C, 1990, *Biomechanics: Motion, Flow, Stress, and Growth*, Springer-Verlag, New York.
5. Gemci, T., T.E. Corcoran, and N. Chigier, 2002. A numerical and experimental study of spray dynamics in a simple throat-model. *Aerosol Science and Technology*, **36**(1):18-38.

6. Gemci, T., B. Shortall, G. Allen, T.E. Corcoran, and N.A. Chigier, 2003. CFD study of the throat during aerosol drug delivery using heliox and air. *Journal of Aerosol Science*, **34**:1175-1192.
7. Guan, X and Martonen, T.B., 2000. Flow Transition in Bends and Applications to Airways. *Journal of Aerosol Science*, **31**(7): 833-847.
8. Horsfield, K., Dart, G., Olson, D.E., and Cumming, G.F., 2002. Models of the human bronchial tree. *Respiratory Physiology & Neurobiology*, **130**:201-221.

9. Hyatt, R.E. and Wilcox, R.E., 1973. The pressure-flow relationship of the intrathoracic airways in man. *J. Clin. Invest.,* **42:** 29-39.
10. Kitaoka, H., Takaki, R., and Suki, B., 1999. A three-dimensional model of the human airway tree. Journal Applied Physiology, **87**(6): 2207-2217.
11. Kleinstreuer, C. and Zhang, Z., 2003. Targeted drug aerosol deposition analysis for a four-generation pulmonary airway model with hemispherical tumors. ASME *Journal of Biomechanical Engineering*, **125**:197-206.
12.Kriete, A., Schmidt, A. H., Zidowitz, S., Haworth, D. C., and Kunz, R. F., 2004. Simulations at a newly derived reference model of the human lung. *Proceedings of SPIE*, Vol. 5318, p. 163-169.
13.Lee, D.Y. and Lee, J.W., 2002. Dispersion of aerosol bolus during one respiration cycle in a model of pulmonary airways. *Journal of Aerosol Science*, **33**:1219-1234.
14. Liu, Y., So, R.M.C., and Zhang, C.H., 2003. Modeling the bifurcating flow in an asymmetric human pulmonary airway. *Journal of Biomechanics*, **36**: 951-959.
15.Nowak, N., Kakade, P.P., and Annapragada, A.V., 2003. Computational fluid dynamics simulation of airflow and aerosol deposition in human lungs. *Annals of Biomedical Engineering*, **31**:374-390.
16.Pedley, T.J., R.C. Schroter, and M.F. Sudlow, 1971. Flow and pressure drop in systems of repeatedly branching tubes. *Journal of Fluid Mechanics*, **46**:365-383.
17.Pedley, T.J. 1977. Pulmonary Fluid Dynamics. *Ann. Rev. Fluid Mech.*, **9:** 229-274.
18. Sauret, V., K.A. Goatman, J.S. Fleming, and A.G. Bailey, 1999. Semiautomated tabulation of the 3D topology and morphology of branching networks using CT: Application to the airway tree. *Physics in Medicine and Biology*, **44**:1625-1638.
19.Schmidt, A., Zidowitz, S., Kriete, A., Denhard, T., Krass, S., and Peitgen, H.-O., 2004. A digital reference model of the human bronchial tree. *Computerized Medical Imaging and Graphics*, **28**:203-211.
20.Sera, T., H. Fujioka, H. Yokota, A. Makinouchi, R. Himeno, R.C. Schroter, and K. Tanishita, 2003. Three-dimensional visualization and morphometry of small airways from microfocal X-ray computed tomography. *Journal of Biomechanics*, **36**:1587-1594.
21. Shi, H., Kleinstreuer, C., and Zhang, Z., 2004. Nanoparticle transport and deposition in bifurcating tubes with different inlet conditions. *Physics of Fluids*, **16**(7):2199-2213.
Snyder, B., Dantzker, D.R., and Jaeger, M.J., 1981. Flow partitioning in symmetric cascades of branches. *Journal of Applied Physiology*, **51**(3):598-506.
22. Spencer, R.M., J.D. Schroeter, and T.B. Martonen, 2001. Computer simulations of pulmonary airway structures using data-driven surface modeling techniques. *Computers in Biology and Medicine*, **31**:499-511.

23. Stapleton, K.W., E. Guentsch, M.K. Hoskinson, and W.H. Finlay, 2000. On the suitability of k-epsilon modeling for aerosol deposition in the mouth and throat: A comparison with experiment. *Journal of Aerosol Science*, **31**:739-749.
24. Tawhai, M.H., A.J. Pullan, and P.J. Hunter, 2000. Generation of an anatomically based three-dimensional model of the conducting airways. *Annals of Biomedical Engineering*, **28**:793-802.
Tawhai, M. H., Hunter, P., Tschirren, J., Reinhardt, J., McLennan, G., and Hoffman, E. A., 2004. CT-based geometry analysis and finite element models of the human and ovine bronchial tree. Journal *Applied Physiology,* **97**(6): 2310-2321.
25. Tgavalekos, N.T., J.G. Venegas, B. Suki, and K.R. Lutchen, 2003. Relation between structure, function, and imaging in a three-dimensional model of the lung. *Annals of Biomedical Engineering*, **31**:363-373.
26. van Ertbruggen, C., Hirsch, C, and Paiva, M., 2005. Anatomically based three-dimensional model of airways to simulate flow and particle transport using computational fluid dynamics. *Journal of Applied Physiology,* **98**(3):970-980.
27. Zhang, Z and Kleinstreuer, C., 2004. Airflow structures and nano-particle deposition in a human upper airway model. *Journal of Computational Physics*, **198**:178-210.
28. Zhang, Z., Kleinstreuer, C., and Kim, C.S., 2002. Cyclic Micron-size Particle Inhalation and Deposition in a Triple Bifurcation Lung Airway Model. *Journal of Aerosol Science*, **33**: 257-281.
Zhao, Y. and Lieber, B.B., 1994. Steady inspiratory flow in a model symmetric bifurcation. *ASME Journal of Biomechanical Engineering*, **116**:488-496.